Beware of cyclic voltammetry! Measurement artefact in accelerated stress test of fuel cell cathode revealed by operando X-ray diffraction

Raphaël Chattot, Marta Mirolo, Isaac Martens, Kavita Kumar, Vincent Martin, Amir Gasmi, Laetitia Dubau, Frédéric Maillard, Luis Castanheira, Jakub Drnec

▶ **To cite this version:**

Raphaël Chattot, Marta Mirolo, Isaac Martens, Kavita Kumar, Vincent Martin, et al.. Beware of cyclic voltammetry! Measurement artefact in accelerated stress test of fuel cell cathode revealed by operando X-ray diffraction. Journal of Power Sources, 2023, 555, pp.232345. 10.1016/j.jpowsour.2022.232345 . hal-03869671

HAL Id: hal-03869671
https://hal.science/hal-03869671

Submitted on 6 Dec 2022

HAL is a multi-disciplinary open access archive for the deposit and dissemination of scientific research documents, whether they are published or not. The documents may come from teaching and research institutions in France or abroad, or from public or private research centers.

L'archive ouverte pluridisciplinaire **HAL**, est destinée au dépôt et à la diffusion de documents scientifiques de niveau recherche, publiés ou non, émanant des établissements d'enseignement et de recherche français ou étrangers, des laboratoires publics ou privés.

Distributed under a Creative Commons Attribution 4.0 International License

Beware of Cyclic Voltammetry! Measurement Artefact in Accelerated Stress Test of Fuel Cell Cathode Revealed by *Operando* X-ray Diffraction

*Raphaël Chattot [1, *], Marta Mirolo [2], Isaac Martens [2], Kavita Kumar [3], Vincent Martin [3], Amir Gasmi [1], Laetitia Dubau [3], Frédéric Maillard [3], Luis Castanheira [4] and Jakub Drnec [2]*

[1] ICGM, Univ. Montpellier, CNRS, ENSCM, 34095 Montpellier Cedex 5, France

[2] ESRF, The European Synchrotron, 71 Avenue des Martyrs, CS40220, 38043 Grenoble Cedex 9, France

[3] Univ. Grenoble Alpes, Univ. Savoie Mont Blanc, CNRS, Grenoble INP*, LEPMI, 38000 Grenoble, France. *Institute of Engineering and Management Univ. Grenoble Alpes

[4] Symbio, 14 Rue Jean-Pierre Timbaud, Espace des Vouillands 2, 38600 Fontaine, France

*e-mail: (RC) raphael.chattot@umontpellier.fr

KEYWORDS: Nanocatalysts, Fuel Cells, Accelerated Stress Test, Cyclic Voltammetry, Operando X-ray Diffraction

ABSTRACT

Efficient screening of proton exchange membrane fuel cell (PEMFC) cathode catalysts long-term stability at the laboratory scale requires the use of accelerated stress tests (ASTs), mostly consisting in cathode potential cycling in the device operational range. However, AST protocols must be complemented with auxiliary *in situ* electrochemical characterization techniques, such as cyclic voltammetry, at least at the beginning and at the end of test. Supposedly non-destructive, such techniques are necessary to interpret the AST in terms of catalyst performance stability.

Here, by combining *operando* X-ray diffraction, on-line inductively coupled plasma mass spectrometry (ICP-MS) and *ex situ* characterization techniques, we provide experimental evidence that the cyclic voltammetry experiment performed at the end of AST controls the increase of the coherent domain size monitored on the aged catalyst. We propose this process originates from a coalescence of crystallites during low potential excursions of the cathode far below the operational range of the device. This study reveals a 'measurement artefact' in typical AST protocols, where the investigated state of the aged catalyst is largely impacted by the cyclic voltammetry measurement itself, without relevance of fuel cell device practical operation.

TEXT

1. Introduction

Cost and durability remain two major barriers to the widespread deployment of proton exchange membrane fuel cell (PEMFC) systems, especially regarding fuel cell electric vehicle application. Because the degradation of the costly platinum group metal(s) (PGM)-based cathode catalyst accounts for most of the system cost and performance decay, a lot of efforts are dedicated to design more efficient and durable cathode catalyst layers [1]. To be competitive, practical PEMFC cathode should (among other prerequisites) exhibit >0.44 A mg_{PGM}^{-1} at 0.9 V cell voltage, with at least 60 % activity retention over 8,000 h of operation (2025 targets from the Fuel Cell Technical Team of the U.S Department of Energy, DoE/FCTT) [2]. To short-cut the duration of such long durability testing by at least two orders of magnitude, accelerated stress tests (ASTs) have been designed to investigate the viability of commercial and experimental catalyst materials in membrane electrode assemblies (MEAs). ASTs typically consist in applying potential/current cycling profiles to the MEA, simulating in a high frequency fashion the electrochemical stress encountered during operation. Despite numerous AST protocols can be found in the literature (including different potential profiles, potential sweep rate, different upper and lower potential limits *etc.* [3–6]) the DoE/FCTT proposed 30,000 square-wave cycles made of potential steps between 0.6 V (3s) and 0.95 V (3s) as a standard protocol (MEA notably operated at 80 °C with hydrogen and nitrogen supplied at the anode and cathode, respectively). However, for the impact of such AST on the cathode catalyst electrocatalytic performance (and to some extents structural) stability to be possibly evaluated, the protocol also includes beginning of test (BoT), end of test (EoT) and intermediate electrochemical characterizations. Such characterizations consist in cell voltage and electric current measurements under reactive gas (polarization curves for activity estimation) and cyclic voltammetry (CV) experiments under inert atmosphere.

Cyclic voltammetry is a powerful tool used as routine technique in numerous fields of electrochemistry, as it probes the redox events occurring at the electrode-electrolyte interface. In case of Pt-based electrodes, measuring the desorption coulometry of under-potentially deposited hydrogen (H_{UPD}) allows (supposing

the maximum surface density of hydrogen adsorbed a known constant) to evaluate the electrochemically active surface area (ECSA) of the electrode. This only requires short time potential excursion(s) of the electrode close to 0 V *vs*. the reversible hydrogen electrode (RHE), typically 0.05 or 0.1 V *vs.* RHE. Because the Pt-based PEMFC anode counter electrode in hydrogen atmosphere can be considered as an RHE under simple experimental conditions, CV experiments can be easily performed directly in the fuel cell device. Supported by the stability of Pt metal observed in the Pourbaix diagram potential-pH range [7], this method is considered as non-destructive. Consequently, CV experiments are an essential part of any AST protocol, since to pass the stability test, the catalyst should retain at least 60% of its initial activity and ECSA according to the DoE/FCTT. This implies ECSA has to be measured by CV experiments at least at BoT and EoT, but additional measurements also after 10, 100, 1k, 3k, 10k and 20k cycles are also recommended.

However, if pure Pt metal is likely the state of the catalyst at the BoT, Pt oxidation and dissolution are well-identified fundamental pillars of catalyst degradation during fuel cell operation and AST [3,6,8–13]. Pt cations can spread within the catalytic layer, being possibly further reduced *in situ* onto metallic nanoparticles according to the Oswald ripening process, or in the polymeric membrane by the crossover hydrogen [14–16]. Thus, considering the aged catalyst state being a combination of Pt in metallic, oxidized and ionic states, the question whether a CV measurement is still a non-destructive tool in regards of these new moieties may deserve more attention. In fact, the same Pourbaix diagram of Pt which supports the stability of Pt metal in a typical CV experiment potential range clearly predicts the reduction of both Pt cations and oxides at potential approaching 0 *vs.* RHE. Most importantly, such low potential excursion of the cathode is not supposed to occur in practical fuel cell operation.

In this contribution, we use a combination of *operando* X-ray diffraction and *ex situ* characterization techniques to investigate the degradation of a Pt/C cathode catalyst in X-ray transparent PEMFC device during a typical AST procedure. The results reveal that, despite the apparently consistent agreement obtained from all the characterization techniques, the degradations observed in typical AST experiment analysis approach are likely misinterpreted. The ‘measurement artefact’ in AST protocols, where the

structure of the aged catalyst is in fact irreversibly modified by the auxiliary CV characterisation tool, is presented and discussed in light of additional fuel cell tests, on-line inductively coupled plasma mass spectrometry (ICP-MS) and *in situ* WAXS measurements in liquid electrolyte.

2. Experimental

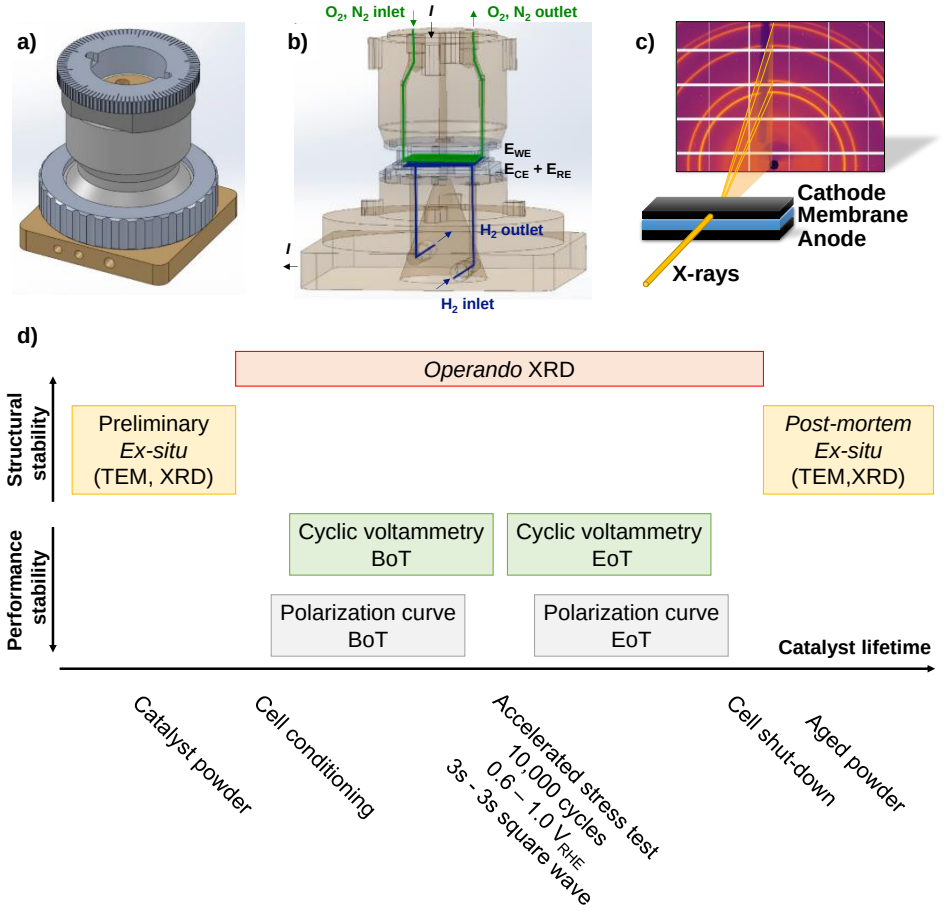

***Figure 1**: Experimental setup and protocol. a-c) X-ray transparent PEMFC for operando WAXS; d) timeline of the different experimental steps and characterization tools used during the catalyst lifetime.*

A commercial 40 wt.% Pt/C catalyst (40 wt. % Pt on medium surface carbon black, ID-n° 5097373, lot EC200840) from Heraeus (Hanau, Germany) was incorporated into 5 cm^2 MEAs (see experimental details in the **Supplementary Material**). For *operando* X-ray diffraction experiments, the MEA was mounted inside an X-ray transparent PEM single cell, described in a dedicated contribution [17] shown in **Figure 1.a-**

b and **Figure S1**. This cell allows the acquisition of wide-angle X-ray scattering (WAXS) patterns of the isolated cathode *operando*, in grazing-incidence configuration (**Figure 1.c**).

The various experimental procedures experienced by the catalyst powder are summarized in the timeline schematic of **Figure 1.d**. After the Pt/C powder catalyst being integrated into a catalyst layer and mounted in the PEMFC, the cell was heated at T = 80 °C and 100 % relative humidity (R.H.), and the anode and cathode sides were fed with 104 sccm H_2 and 250 sccm O_2 gas, respectively, with 0.5 bar backpressure (1.5 bar absolute). The cell was conditioned *via* a short protocol (considering limited allocated beamtime) consisting in 5 repetitions of a potential cycle composed of 2 min at open circuit voltage (OCP), followed by 3 min at cell voltage of 0.85 V and 10 min at 0.65 V. Then, a BoT polarization curve consisting of 10 current density steps between 0 and 1 A cm^{-2} was performed, and the cell voltage was measured after 3 min of stabilization at each step. During the polarization curve, the O_2 stoichiometry was maintained at 9.5, while the H_2 flow was kept constant (104 sccm, corresponding to a stoichiometry of 3 at 1 A cm^{-2}). Afterwards, O_2 gas at cathode was replaced by 250 sccm N_2, and BoT CVs (3 cycles between 0.05 and 1.0 V *vs.* RHE at a potential sweep rate of 50 mV s^{-1}) were recorded. The core of the AST consisted in 10,000 square-wave cycles made of potential steps between 0.6 (3s) and 1.0 V *vs.* RHE (3s) under N_2 cathode gas atmosphere. Importantly, for each WAXS measurement (frequency of the measurements being shown later) the potential cycling was interrupted and the cathode was maintained at E = 0.4 V *vs.* RHE during WAXS acquisition (for *ca* 5 min). Finally, EoT characterizations consisted in EoT CV in N_2 cathode atmosphere (as CV BoT) followed by EoT polarization under O_2 cathode atmosphere (as BoT polarisation curve). The cell was eventually turned off, and the aged MEA kept for further *post mortem* analysis. The same experiment protocol was also conducted in a 'conventional' single PEMFC (see picture in **Figure S1**) at the laboratory scale without *operando* WAXS measurements (see the **Supplementary Material)**. Finally, complementary on-line inductively coupled plasma mass spectrometry (ICP-MS) and *in situ* WAXS measurements in liquid electrolyte were also performed, as introduced later and described in the **Supplementary Material**).

3. Results and Discussion

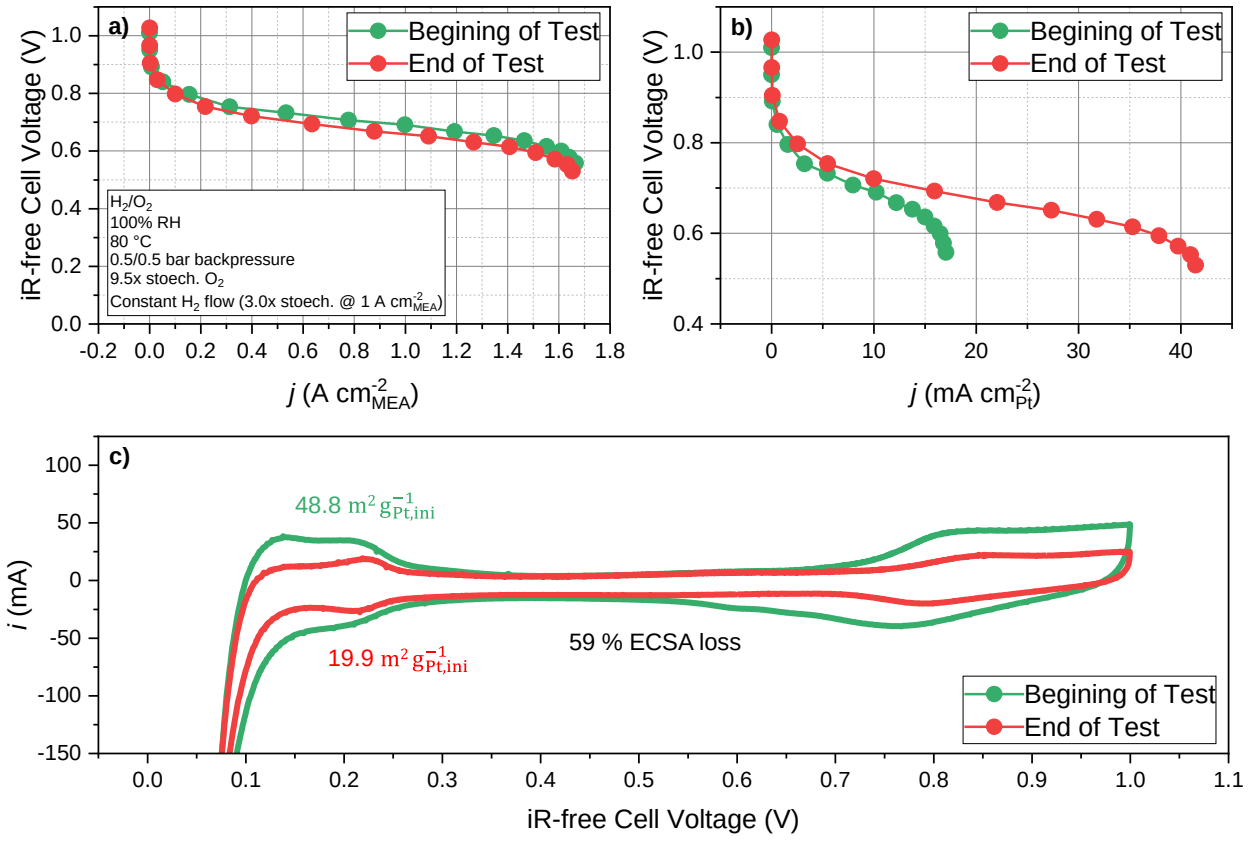

***Figure 2**: BoT and EoT electrochemical data in the conventional laboratory fuel cell. a) geometric surface area normalized current-voltage polarization curves, b) Pt surface area normalized current-voltage polarization curves and c) cyclic voltammograms recorded at 50 mV s^{-1}. In c), the Pt surface area (ECSA) is calculated by H_{UPD} coulometry. Cathode loading: 0.2 mg_{Pt} cm^{-2}.*

Because the X-ray transparent fuel cell is not optimized for high performance, **Figure 2.a-b** shows the cell performance measured at BoT and EoT in the conventional cell (results from the X-ray transparent cell are displayed in **Figure S2**). **Figure 2.a** clearly reveals the detrimental impact of the AST on the catalyst

activity, as a negative shift of *ca* 35 mV at 1 A cm_{MEA}^{-2} is observed in the polarization curve. The CVs recorded at BoT and EoT in **Figure 2.c**, likely provide the cause of such performance decrease. From H_{UPD} coulometry, the AST caused nearly 60% of ECSA loss. Interestingly, normalizing the cell performance by the ECSA in **Figure 2.b** highlights an increase of the Pt specific activity after the AST. Such opposite trends in mass- (or geometric) activity *vs.* specific activity can be explained at least partially by an increase of the nanoparticle size during ageing [18]. Importantly, despite the performance being different from one cell to the other, an excellent agreement is obtained for the ECSA trend, as shown in **Table 1**. Moreover, the Pt specific surface area of 47.2 or 48.8 m^2 $g_{Pt,ini}^{-1}$ measured at BoL in the two PEMFC approaches the value of 56 m^2 g_{Pt}^{-1} measured during a control experiment in liquid electrolyte for the same catalyst (not shown). Ensuring a near-complete electrode-electrolyte contact from the catalyst layer is essential for further consistent interpretation of such AST.

Table 1: Evolution of the ECSA measured by H_{UPD} coulometry at BoT and EoT in the two PEMFC used.

	X-ray transparent PEMFC	**Conventional PEMFC**
ECSA BoT	47.2 m^2 g_{Pt}^{-1}	48.8 m^2 g_{Pt}^{-1}
ECSA EoT	19.2 m^2 g_{Pt}^{-1}	19.9 m^2 g_{Pt}^{-1}
ECSA loss	59 %	59 %

More insights on the origin of ECSA loss can be obtained from preliminary and *post mortem* analyses of the materials aged in the X-ray transparent cell. Both the fresh catalyst powder and aged catalyst powder collected from the tested MEA were investigated with TEM and *ex situ* WAXS (see experimental details in the **Supplementary Material**). As shown in **Figure 3**, these two techniques indicate an important increase of the nanoparticle size and coherent domain size, respectively. Rietveld refinement of the WAXS patterns gives a coherent domain size increasing from 3.7 nm at BoT to 9.7 nm at EoT (**Figure 3.a**), very

close to the volume-averaged particle size found by TEM (from 3.8 nm to 13.0 nm). Note that only the volume-averaged TEM sizes can be tentatively compared to the volume-sensitive WAXS, and that coherent domain size is a slightly distinct notion from nanoparticle geometric size. Furthermore, estimating nanoparticle size on the aged catalyst accurately from very local TEM images is a difficult if not impossible task considering the presence of aggregates and broad size distribution. Supposing cuboctahedral shape for the crystallites, it is possible to estimate the Pt specific surface areas at BoT and EoT from the WAXS coherent domain sizes [19]. The values of 66 m^2 g_{Pt}^{-1} and 29 m^2 g_{Pt}^{-1} for BoT and EoT, respectively, are significantly higher than the values of 47.2 m^2 g_{Pt}^{-1} and 19.2 m^2 $g_{Pt,ini}^{-1}$ derived from ECSA measurements, which can be likely explained by both particles aggregation and contact areas with the carbon support (included in the WAXS values but not necessarily electrochemically accessible).

Interestingly, however, a theoretical Pt specific surface area loss of 56 % is predicted from the nanoparticle coherent domain size increase, in excellent agreement with the measured ECSA loss of 59 %. This suggests that 95 % of the ECSA loss can be accounted for particle size increase, with no or only few losses of Pt metal mass. These results are consistent with numerous previous reports on Pt/C degradation in PEMFC [14–16,20], which highlighted the limited time existence of Pt^{z+} ions in operating PEMFC MEAs due to various redeposition processes [21]. Regarding the amplitude in particle size increase, reaching *ca* 10 nm after degradation tests in PEMFC is also quite typical. Martens *et al.*, [22] reached 10.3 nm from commercial Pt/C MEA in similar conditions after 10,000 triangular wave AST between 0.6 V *vs.* RHE and 1.0 V *vs.* RHE at 50 mV s^{-1}. Similar particle size values were obtained also with different experimental conditions, such as potential cycling to different upper potential limits, different amount of cycles or even after extensive operation at constant current load [14–16,20,23].

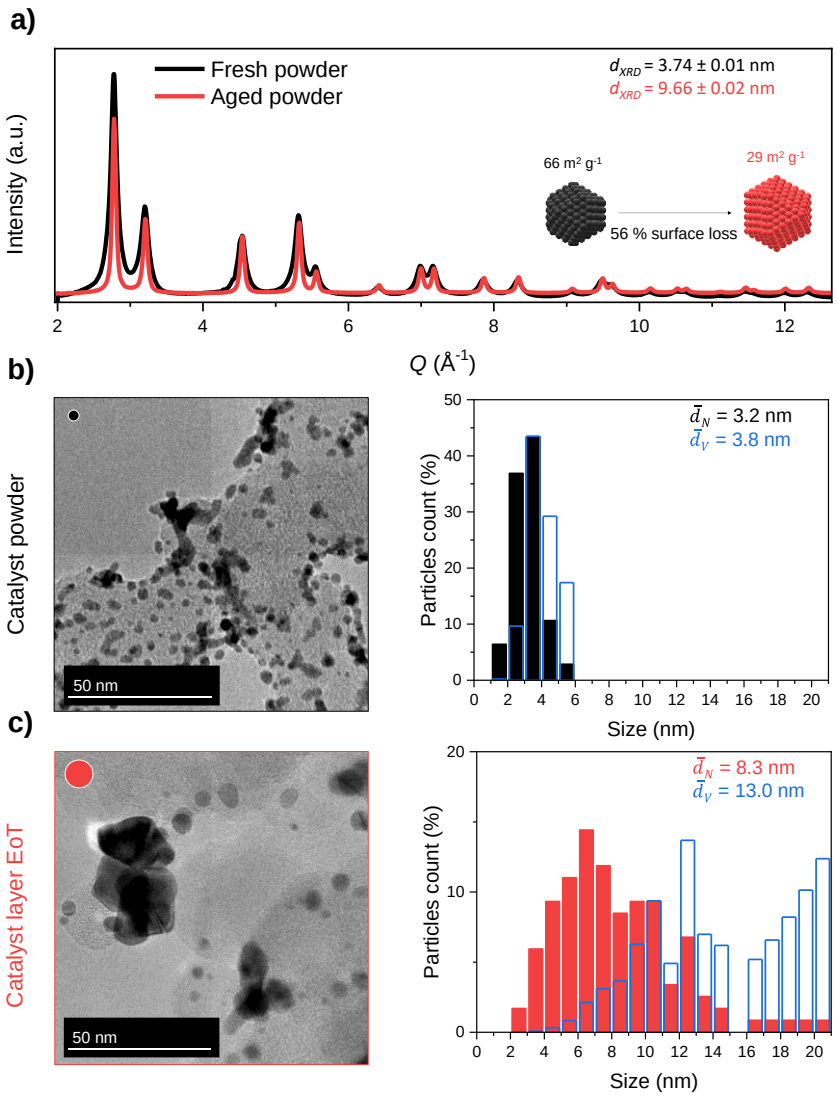

***Figure 3**: BoT and EoT ex situ characterizations. a) WAXS patterns with corresponding coherent domain size extracted from Rietveld refinement and Pt specific surface areas. TEM images with corresponding number- and volume-averaged particle size distributions at b) BoT and c) EoT, respectively. On the TEM images, top left corners in b) and c), circles scale with the volume-averaged distribution mean are displayed.*

We now present the WAXS data measured *operando* over the course of the complete AST protocol. WAXS patterns were collected in grazing incidence configuration as represented in **Figure 1.c**. Importantly, the full MEA was scanned vertically by the X-ray beam from the anode to the cathode, and the WAXS patterns from the cathode were averaged for a complete capture of the degradation over the catalyst layer thickness

[24]. WAXS was measured between each experimental step, and after different amounts of cycles during the AST. **Figure 4** shows the evolution of the coherent domain size over the course of the complete AST protocol. Strikingly, if the coherent domain size values from *operando* WAXS measurements agree with the values found *ex situ* at BoT and EoT, they reveal the observed coherent domain size increase mainly originates from the cyclic voltammetry experiment performed after the AST (from 4.3 nm to 10.4 nm), and not from the AST itself (from 3.8 nm to 4.3 nm). Closer look on the AST cycles in **Figure 4.b** shows that the AST cycles did induce a sharp coherent domain size increase during the first 1,000 cycles, but was followed by a much slower evolution for the rest of the test (as also previously observed [22,25,26]). To discard any experimental artefact possibly altering the results observed during the *operando* WAXS experiment (electrode potential control loss or beam damage), we performed *ex situ* X-ray diffraction (XRD) from laboratory source (see details in the **Supplementary Material**) on pristine and aged GDEs in the conventional laboratory cell with and without EoT CV experiment after the AST. As shown in **Figure 4.a**, the Scherrer formula applied on these independent measurements (see **Figure S3**) reveals an evolution of the coherent domain size from 4.01 nm to 5.87 nm or 9.04 nm after AST or after AST and EoT CV experiment, respectively, in agreement with the *operando* WAXS. This unambiguously reveals the detrimental, and largely overlooked impact a simple CV experiment can have on an aged catalyst sample (note the CV recorded at the BoT had no such impact). We argue that such dramatic changes must be caused by the strong reducing conditions experienced by the aged catalyst layer once its potential is swept in the H_{UPD} region for ECSA measurement. The critical potential limit triggering this process is unfortunately not known at this stage, but it must be below E = 0.4 V *vs.* RHE, considering the WAXS measurements in **Figure 4.b** were performed at this potential, and as confirmed below.

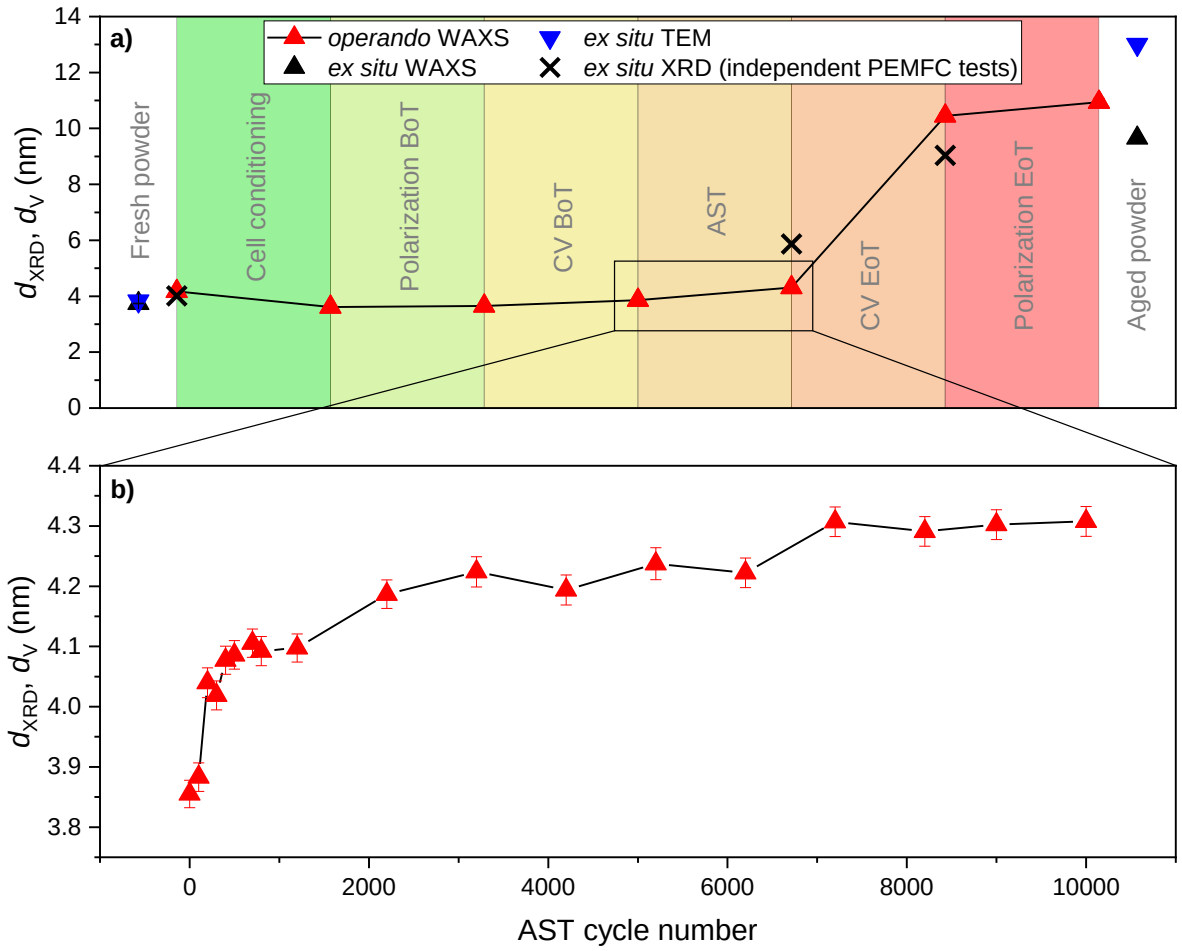

***Figure 4**: Coherent domain size extracted from Rietveld measurement of the WAXS patterns measured ex situ (black markers) and operando (red markers), volume-averaged particle size estimated by TEM ex situ (blue markers) and coherent domain size estimated with the Scherrer formula from ex situ laboratory XRD performed on independent PEMFC tests. Operando WAXS was measured between a) each experimental step and b) after different amounts of cycles during the AST.*

The observed coherent domain size increase could originate from a combination of (i) redeposition of Pt ions onto pre-existing crystalline nanoparticles, (ii) reduction of amorphous Pt oxides to a crystalline Pt metal form, or (iii) coalescence of polycrystalline aggregates to monocrystalline nanoparticles. Regarding the first possibility, and as discussed earlier, the presence of Pt cations in high concentration at potentials as low as 0.4 V *vs.* RHE is thermodynamically impossible in the presence of *ca.* 4 nm Pt nanoparticles [27]. The second possibility (*i.e.* the sudden reduction of amorphous Pt surface oxide below $E = 0.4$ V *vs.* RHE)

is verified here by on-line ICP-MS measurements. Pt dissolution from the same Pt/C catalyst during cyclic voltammetry experiments in 0.1 M $HClO_4$ electrolyte was monitored at room temperature during cyclic voltammetry experiments between 0.05 and 1.23 V vs. RHE at 5 mV s^{-1}. As shown in **Figure 5.a-b**, the potential-resolved Pt dissolution profile (blue trace in **Figure 5.b**) shows three main contributions per cycle. The first two dissolution peaks, referred as A_1 and C_1 correspond to well-known anodic and cathodic processes, respectively [12]. A_1 is triggered by the formation of Pt oxides when the potential exceeds *ca* 0.9 V *vs.* RHE and C_1 by the reduction of Pt oxides when the potential is decreased below *ca* 1.0 V vs. RHE. Interestingly, the present on-line ICP-MS data (but in fact also others [11,12]) clearly allows the identification of a second cathodic dissolution process, labelled C_2, when the potential is further decreased below *ca* 0.35 V *vs.* RHE. By extension of the mechanism ruling C_1, we argue the presence of C_2 is an indirect detection of the reduction of Pt surface oxides occurring a such low electrode potential. Since C_2 is about 40 times less intense than C_1, the amount of such remaining surface oxides must be significantly low. Synchronization of the on-line ICP-MS data with *in situ* WAXS data measured in similar conditions (but with a potential sweep rate of 20 mV s^{-1}) displayed in **Figure 5.c** reveals C_2 occurs just before and during the adsorption of hydrogen (monitored by the lattice strain increase [28]). Interestingly, the C_2 process seems to be magnified during the first of the three cycles recorded, suggesting it is highly sensitive to the history of the electrode. In **Figure 5**, the electrode was equilibrated at E = 0.4 V vs. RHE before performing the measurements. In the case of post-AST, aged catalyst, the amount of Pt oxides is likely even higher. In fact, and as shown in **Figure S4**, a mild additional reducing current contribution can be observed on the cyclic voltammograms during the first excursion at low electrode potential only at EoT. The present hypothesis is also supported by a previous contribution from Sandbeck *et al.* [29], which identified from online ICP-MS dissolution profiles the lower potential limit of 0.6 V *vs.* RHE being too much positive in typical AST procedure to fully reduce Pt oxides on 4 nm nanoparticles.

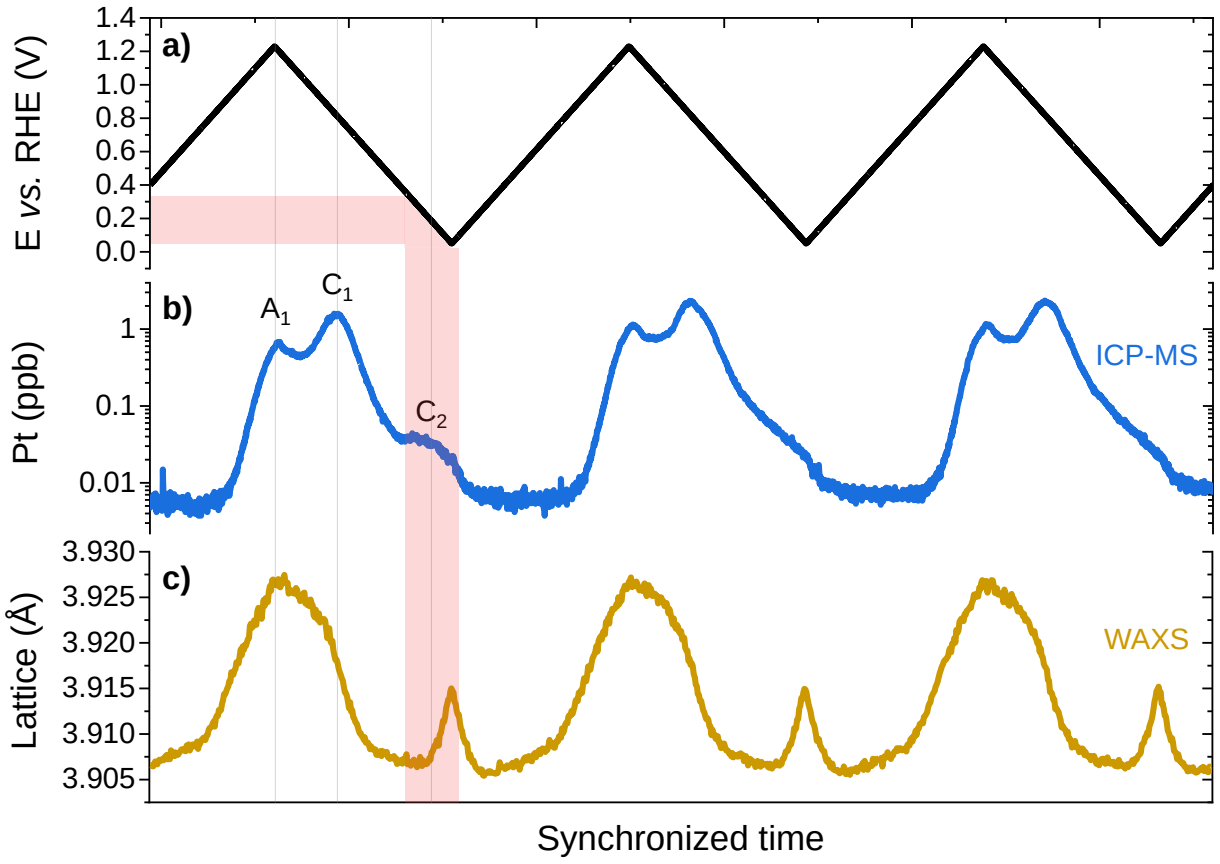

***Figure 5**: Online inductively-coupled plasma mass spectrometry (ICP-MS) and in situ WAXS data measured during cyclic voltammetry experiments in 0.1 M $HClO_4$ electrolyte. The potential profile in a) is valid for both the on-line ICP-MS and WAXS data in b) and c), respectively. The red boxes are displayed to guide the eyes in the identification of the C_2 dissolution process.*

If these extra measurements in liquid electrolyte support the possibility of highly oxophilic Pt sites reduction occurring only at low electrode potential, this can hardly explain on its own such particle size increase. In fact, based on a cuboctahedral shape model [19], Pt nanocrystallites of 4.3 nm and 10.4 nm (before and after EoT CVs) are composed of *ca* 3,000 and 40,000 atoms, respectively. This means, *ca* 92 % of the total Pt mass in the form of Pt^{z+} cations or amorphous oxide surface layer would be needed to produce such a nanoparticle coherent domain size increase after reduction/redeposition, which seems unrealistic. The last

possibility among the above-mentioned causes of coherent domain size increase is the sudden coalescence of aggregates. In contrast to the other possibilities discussed, such scenario could easily explain the *ca* 2.3-fold size increase observed here. In a recent contribution [25], Martens *et al.* monitored *operando* the particle size increase of a commercial Pt/C catalyst over the course of an AST in PEMFC with wide- and small-angle X-ray scattering (WAXS *vs.* SAXS). The complementary sensitivities of the techniques regarding the particle size definition (coherent domain size *vs.* geometric size for WAXS and SAXS, respectively) allowed to clearly identify the aggregation process as anterior to the coalescence process in the overall degradation mechanism. Moreover, hydrogen adsorption is well-known to enhance Pt surface reconstruction [30] and nanoparticle sintering under thermal treatment [31,32] or in electrochemical environment [33]. Thus, from the available literature and the data of this contribution, we propose the following simple mechanism to covertly 'corrupt' standardized AST protocols (**Figure 6**): (i) the core of the AST (cycling between $0.6 \leq E \leq 1.0$ V vs. RHE) indeed triggers the well-known Pt degradation processes (Pt dissolution, nanoparticles aggregation and growth according to the Ostwald ripening process, **Figure 6.a**), (ii) the surface state reached after the potential cycling above 0.6 V vs. RHE is still partially oxidized; (iii) electrode excursion to reducing potentials of the 'H_{UPD} region' during ECSA measurement at EoT reduces Pt surface oxides while hydrogen adsorption enhance Pt atoms surface diffusion and coalescence of aggregates (**Figure 6.b**).

Finally, if the present study reports a quite consequent structural transformation caused by the cyclic voltammetry experiment performed at the EoT, the coherent domain size increase must be correctly interpreted. The nanoparticles do not simply grow from *ca* 4 nm to *ca* 10 nm, but aggregates formed during the AST coalesce during the EoT CV experiment. If the impact of such coalescence on the ECSA value cannot be easily accessed (at least not by conventional CV experiment), polarization curves measured after the AST but before and after the EoT CV experiment in **Figure S5** reveal a possible minor positive impact of the coalescence on the cell performance in this case. Note, however, the conclusions could be different if the CV experiments are performed regularly after various amounts of cycles as recommended by the

DoE/FCTT. In fact, Castanheira *et al.* [34] reported that implementing intermediate characterizations (CVs and CO_{ads} stripping experiments) during a 96 h potentiostatic hold at E =1.0 V vs. RHE AST results in a 3.5-fold magnification of ECSA loss compared to the AST alone.

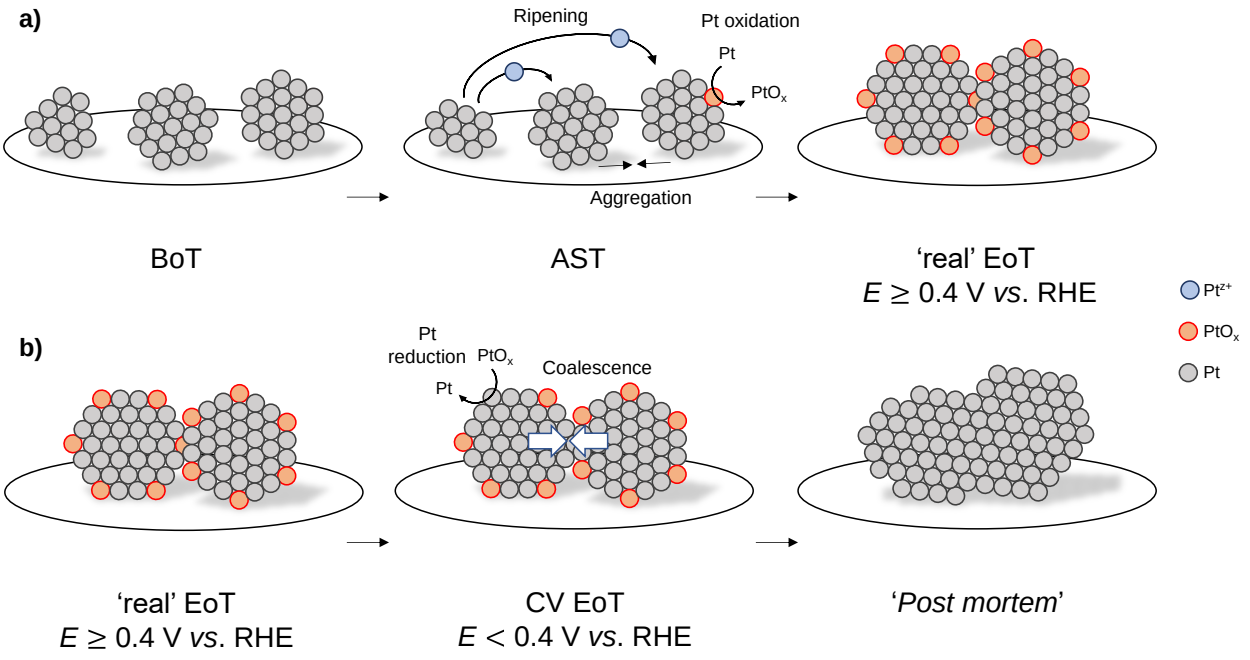

***Figure 6**: Proposed mechanism highlighting the structural and chemical changes occurring during a) the core of the AST and b) the EoT CV experiment. The only few amounts of Pt oxides represented after AST refers to the oxides still present at E = 0.4 V vs. RHE, and further reduced during the EoT CV experiment.*

CONCLUSIONS

In this contribution, we used *operando* X-ray diffraction to capture the dramatic impact of cyclic voltammetry experiments on the structure of a Pt/C catalyst when performed on degraded (aged) fuel cell catalyst layer. Our observations, confirmed by a replica of the experiment, reveal that the cyclic voltammetry measurement performed at the end of a typical AST procedure causes more coherent domain size increase than the AST itself. Thus, despite being a very convenient tool to probe the catalyst structure *in situ*, the admitted non-destructive property of this technique on pristine (metallic) catalysts does not seem to hold upon catalyst degradation. The 2-3-fold increase in coherent domain size observed after cycling to

low electrode potentials suggests a lightning coalescence of aggregated nanoparticles, triggered by the reduction of Pt oxides. Since the cyclic voltammetry experiments in the context of ASTs are used to determine the electrochemically active surface area of the catalyst, the question whether this measurement remains valid considering the structural changes it causes is now open, and alternative catalyst performance/structural assessment metrics may be needed.

AUTHOR INFORMATION

Corresponding Author

Raphaël Chattot, ICGM, Univ. Montpellier, CNRS, ENSCM, 34095 Montpellier Cedex 5, France.

https://orcid.org/0000-0001-6169-530X ; email : raphael.chattot@umontpellier.fr

ACKNOWLEDGEMENTS

We would like to thank ESRF for the provision of the beamtime at ID31 beamline as well as Helena Isern and Florian Russello for the help with the beamline preparation. R.C gratefully acknowledge financial support from the French National Research Agency through the HOLYCAT project (grant number n◦ ANR-22-CE05-0007) and Dr. Bernard Fraisse from the analysis and characterisation platform of the Pôle Chimie Balard. L.C., , K.K, V. M, F.M. and L.D. gratefully acknowledge financial support from the French National Research Agency through the BRIDGE project (grant number n◦ANR-19-ENER-0008-01).

REFERENCES

(1) Kodama, K.; Nagai, T.; Kuwaki, A.; Jinnouchi, R.; Morimoto, Y. Challenges in Applying Highly Active Pt-Based Nanostructured Catalysts for Oxygen Reduction Reactions to Fuel Cell Vehicles. *Nat. Nanotechnol.* **2021**, *16* (2), 140–147. https://doi.org/10.1038/s41565-

020-00824-w.

(2) Abdel-Baset, T.; Benjamin, T.; Borup, R.; Martin, K. E.; Garland, N.; Hirano, S.; Kopasz, J.; Lakshmanmn, B.; Masten, D.; Mehall, M.; Myers, D.; Papageorgopoulos, D.; Podolski, W.; Trabold, T.; Vermeersch, B.; Waldecker, J. *The Fuel Cell Technical Team Roadmap*; 2017. https://doi.org/10.2172/1220127.

(3) Stariha, S.; Macauley, N.; Sneed, B. T.; Langlois, D.; More, K. L.; Mukundan, R.; Borup, R. L. Recent Advances in Catalyst Accelerated Stress Tests for Polymer Electrolyte Membrane Fuel Cells. *J. Electrochem. Soc.* **2018**, *165* (7), F492–F501. https://doi.org/10.1149/2.0881807jes.

(4) Zhang, H.; Haas, H.; Hu, J.; Kundu, S.; Davis, M.; Chuy, C. The Impact of Potential Cycling on PEMFC Durability. *J. Electrochem. Soc.* **2013**, *160* (8), F840–F847. https://doi.org/10.1149/2.083308jes.

(5) Borup, R. L.; Kusoglu, A.; Neyerlin, K. C.; Mukundan, R.; Ahluwalia, R. K.; Cullen, D. A.; More, K. L.; Weber, A. Z.; Myers, D. J. Recent Developments in Catalyst-Related PEM Fuel Cell Durability. *Curr. Opin. Electrochem.* **2020**, *21*, 192–200. https://doi.org/10.1016/j.coelec.2020.02.007.

(6) Uchimura, M.; Sugawara, S.; Suzuki, Y.; Zhang, J.; Kocha, S. S. Electrocatalyst Durability under Simulated Automotive Drive Cycles. *ECS Trans.* **2008**, *16* (2), 225–234. https://doi.org/10.1149/1.2981858.

(7) Pourbaix, M. *Atlas of Electrochemical Equilibria in Aqueous Solutions*; National association of Corrosion Engineers, Ed.; 1974. https://doi.org/10.4028/www.scientific.net/msf.251-254.143.

(8) Topalov, A. A.; Cherevko, S.; Zeradjanin, A. R.; Meier, J. C.; Katsounaros, I.; Mayrhofer,

K. J. J. Towards a Comprehensive Understanding of Platinum Dissolution in Acidic Media. *Chem. Sci.* **2014**, *5* (2), 631–638. https://doi.org/10.1039/c3sc52411f.

(9) Fuchs, T.; Drnec, J.; Calle-Vallejo, F.; Stubb, N.; Sandbeck, D. J. S.; Ruge, M.; Cherevko, S.; Harrington, D. A.; Magnussen, O. M. Structure Dependency of the Atomic-Scale Mechanisms of Platinum Electro-Oxidation and Dissolution. *Nat. Catal.* **2020**, *3* (9), 754–761. https://doi.org/10.1038/s41929-020-0497-y.

(10) Lopes, P. P.; Li, D.; Lv, H.; Wang, C.; Tripkovic, D.; Zhu, Y.; Schimmenti, R.; Daimon, H.; Kang, Y.; Snyder, J.; Becknell, N.; More, K. L.; Strmcnik, D.; Markovic, N. M.; Mavrikakis, M.; Stamenkovic, V. R. Eliminating Dissolution of Platinum-Based Electrocatalysts at the Atomic Scale. *Nat. Mater.* **2020**, *19* (11), 1207–1214. https://doi.org/10.1038/s41563-020-0735-3.

(11) Sandbeck, D. J. S.; Sandbeck, D. J. S.; Inaba, M.; Quinson, J.; Bucher, J.; Zana, A.; Arenz, M.; Arenz, M.; Cherevko, S. Particle Size Effect on Platinum Dissolution: Practical Considerations for Fuel Cells. *ACS Appl. Mater. Interfaces* **2020**, *12* (23), 25718–25727. https://doi.org/10.1021/acsami.0c02801.

(12) Kasian, O.; Geiger, S.; Mayrhofer, K. J. J.; Cherevko, S. Electrochemical On-Line ICP-MS in Electrocatalysis Research. *Chem. Rec.* **2019**, *19* (10), 2130–2142. https://doi.org/10.1002/tcr.201800162.

(13) Ehelebe, K.; Seeberger, D.; Paul, M. T. Y.; Thiele, S.; Mayrhofer, K. J. J.; Cherevko, S. Evaluating Electrocatalysts at Relevant Currents in a Half-Cell: The Impact of Pt Loading on Oxygen Reduction Reaction. *J. Electrochem. Soc.* **2019**, *166* (16), F1259–F1268. https://doi.org/10.1149/2.0911915jes.

(14) Borup, R.; Meyers, J.; Pivovar, B.; Kim, Y. S.; Mukundan, R.; Garland, N.; Myers, D.;

Wilson, M.; Garzon, F.; Wood, D.; Zelenay, P.; More, K.; Stroh, K.; Zawodzinski, T.; Boncella, J.; McGrath, J. E.; Inaba, M.; Miyatake, K.; Hori, M.; Ota, K.; Ogumi, Z.; Miyata, S.; Nishikata, A.; Siroma, Z.; Uchimoto, Y.; Yasuda, K.; Kimijima, K. I.; Iwashita, N. Scientific Aspects of Polymer Electrolyte Fuel Cell Durability and Degradation. *Chem. Rev.* **2007**, *107* (10), 3904–3951. https://doi.org/10.1021/cr050182l.

(15) De Bruijn, F. A.; Dam, V. A. T.; Janssen, G. J. M. Review: Durability and Degradation Issues of PEM Fuel Cell Components. *Fuel Cells* **2008**, *8* (1), 3–22. https://doi.org/10.1002/fuce.200700053.

(16) Dubau, L.; Castanheira, L.; Maillard, F.; Chatenet, M.; Lottin, O.; Maranzana, G.; Dillet, J.; Lamibrac, A.; Perrin, J. C.; Moukheiber, E.; Elkaddouri, A.; De Moor, G.; Bas, C.; Flandin, L.; Caqué, N. A Review of PEM Fuel Cell Durability: Materials Degradation, Local Heterogeneities of Aging and Possible Mitigation Strategies. *Wiley Interdiscip. Rev. Energy Environ.* **2014**, *3* (6), 540–560. https://doi.org/10.1002/wene.113.

(17) Martens, I.; Vamvakeros, A.; Chattot, R.; Blanco, M. V.; Rasola, M.; Pusa, J.; Jacques, S. D. M.; Bizzotto, D.; Wilkinson, D. P.; Ruffmann, B.; Heidemann, S.; Honkimäki, V.; Drnec, J. X-Ray Transparent Proton-Exchange Membrane Fuel Cell Design for in Situ Wide and Small Angle Scattering Tomography. *J. Power Sources* **2019**, *437*. https://doi.org/10.1016/j.jpowsour.2019.226906.

(18) Perez-Alonso, F. J.; McCarthy, D. N.; Nierhoff, A.; Hernandez-Fernandez, P.; Strebel, C.; Stephens, I. E. L.; Nielsen, J. H.; Chorkendorff, I. The Effect of Size on the Oxygen Electroreduction Activity of Mass-Selected Platinum Nanoparticles. *Angew. Chemie - Int. Ed.* **2012**, *51* (19), 4641–4643. https://doi.org/10.1002/anie.201200586.

(19) Montejano-Carrizales, J. M.; Aguilera-Granja, F.; Morán-López, J. L. Direct Enumeration

of the Geometrical Characteristics of Clusters. *Nanostructured Mater.* **1997**, *8* (3), 269–287. https://doi.org/10.1016/S0965-9773(97)00168-2.

(20) Weiß, A.; Siebel, A.; Bernt, M.; Shen, T.-H.; Tileli, V.; Gasteiger, H. A. Impact of Intermittent Operation on Lifetime and Performance of a PEM Water Electrolyzer. *J. Electrochem. Soc.* **2019**, *166* (8), F487–F497. https://doi.org/10.1149/2.0421908jes.

(21) Dubau, L.; Castanheira, L.; Maillard, F.; Chatenet, M.; Lottin, O.; Maranzana, G.; Dillet, J.; Lamibrac, A.; Perrin, J. C.; Moukheiber, E.; Elkaddouri, A.; De Moor, G.; Bas, C.; Flandin, L.; Caqué, N. A Review of PEM Fuel Cell Durability: Materials Degradation, Local Heterogeneities of Aging and Possible Mitigation Strategies. *Wiley Interdiscip. Rev. Energy Environ.* **2014**, *3* (6), 540–560. https://doi.org/10.1002/wene.113.

(22) Martens, I.; Vamvakeros, A.; Martinez, N.; Chattot, R.; Pusa, J.; Blanco, M. V.; Fisher, E. A.; Asset, T.; Escribano, S.; Micoud, F.; Starr, T.; Coelho, A.; Honkimäki, V.; Bizzotto, D.; Wilkinson, D. P.; Jacques, S. D. M.; Maillard, F.; Dubau, L.; Lyonnard, S.; Morin, A.; Drnec, J. Imaging Heterogeneous Electrocatalyst Stability and Decoupling Degradation Mechanisms in Operating Hydrogen Fuel Cells. *ACS Energy Lett.* **2021**, *6* (8), 2742–2749. https://doi.org/10.1021/acsenergylett.1c00718.

(23) Shokhen, V.; Skoglundh, M. Impact of Accelerated Stress Tests on the Cathodic Catalytic Layer in a Proton Exchange Membrane (PEM) Fuel Cell Studied by Identical Location Scanning Electron Microscopy. **2022**. https://doi.org/10.1021/acsaem.2c01790.

(24) Schröder, J.; Pittkowski, R. K.; Martens, I.; Chattot, R.; Drnec, J.; Quinson, J.; Kirkensgaard, J. J. K.; Arenz, M. Tracking the Catalyst Layer Depth-Dependent Electrochemical Degradation of a Bimodal Pt/C Fuel Cell Catalyst: A Combined Operando Small- and Wide-Angle X-Ray Scattering Study. *ACS Catal.* **2022**, *12* (3), 2077–2085.

https://doi.org/10.1021/acscatal.1c04365.

(25) Martens, I.; Chattot, R.; Drnec, J. Decoupling Catalyst Aggregation, Ripening, and Coalescence Processes inside Operating Fuel Cells. *J. Power Sources* **2022**, *521*, 230851. https://doi.org/10.1016/j.jpowsour.2021.230851.

(26) Hornberger, E.; Merzdorf, T.; Schmies, H.; Hübner, J.; Klingenhof, M.; Gernert, U.; Kroschel, M.; Anke, B.; Lerch, M.; Schmidt, J.; Thomas, A.; Chattot, R.; Martens, I.; Drnec, J.; Strasser, P. Impact of Carbon N-Doping and Pyridinic-N Content on the Fuel Cell Performance and Durability of Carbon-Supported Pt Nanoparticle Catalysts. *ACS Appl. Mater. Interfaces* **2022**. https://doi.org/10.1021/acsami.2c00762.

(27) Redmond, E. L.; Setzler, B. P.; Juhas, P.; Billinge, S. J. L.; Fuller, T. F. In-Situ Monitoring of Particle Growth at PEMFC Cathode under Accelerated Cycling Conditions. *Electrochem. Solid-State Lett.* **2012**, *15* (5), 72–75. https://doi.org/10.1149/2.004206esl.

(28) Chattot, R.; Martens, I.; Mirolo, M.; Ronovsky, M.; Russello, F.; Isern, H.; Braesch, G.; Hornberger, E.; Strasser, P.; Sibert, E.; Chatenet, M.; Honkimäki, V.; Drnec, J. Electrochemical Strain Dynamics in Noble Metal Nanocatalysts. *J. Am. Chem. Soc.* **2021**, *143* (41), 17068–17078. https://doi.org/10.1021/jacs.1c06780.

(29) Sandbeck, D. J. S.; Secher, N. M.; Speck, F. D.; Sørensen, J. E.; Kibsgaard, J.; Chorkendorff, I.; Cherevko, S. Particle Size Effect on Platinum Dissolution: Considerations for Accelerated Stability Testing of Fuel Cell Catalysts. *ACS Catal.* **2020**, *10* (11), 6281–6290. https://doi.org/10.1021/acscatal.0c00779.

(30) Horch, S.; Lorensen, H. T.; Helveg, S.; Lægsgaard, E.; Stensgaard, I.; Jacobsen, K. W.; Nørskov, J. K.; Besenbacher, F. Enhancement of Surface Self-Disfusion of Platinum Atoms by Adsorbed Hydrogen. *Nature* **1999**, *398* (6723), 134–136. https://doi.org/10.1038/18185.

(31) Fiedorow, R. M. J.; Chahar, B. S.; Wanke, S. E. The Sintering of Supported Metal Catalysts. II. Comparison of Sintering Rates of Supported Pt, Ir, and Rh Catalysts in Hydrogen and Oxygen. *J. Catal.* **1978**, *51* (2), 193–202. https://doi.org/10.1016/0021-9517(78)90293-2.

(32) Dubau, L.; Nelayah, J.; Moldovan, S.; Ersen, O.; Bordet, P.; Drnec, J.; Asset, T.; Chattot, R.; Maillard, F. Defects Do Catalysis: CO Monolayer Oxidation and Oxygen Reduction Reaction on Hollow PtNi/C Nanoparticles. *ACS Catal.* **2016**, *6* (7), 4673–4684. https://doi.org/10.1021/acscatal.6b01106.

(33) McCrum, I. T.; Bondue, C. J.; Koper, M. T. M. Hydrogen-Induced Step-Edge Roughening of Platinum Electrode Surfaces. *J. Phys. Chem. Lett.* **2019**, *10* (21), 6842–6849. https://doi.org/10.1021/acs.jpclett.9b02544.

(34) Castanheira, L.; Dubau, L.; Maillard, F. Accelerated Stress Tests of Pt/HSAC Electrocatalysts: An Identical-Location Transmission Electron Microscopy Study on the Influence of Intermediate Characterizations. *Electrocatalysis* **2014**, *5* (2), 125–135. https://doi.org/10.1007/s12678-013-0173-y.

TABLE OF CONTENTS/ABSTRACT GRAPHICS

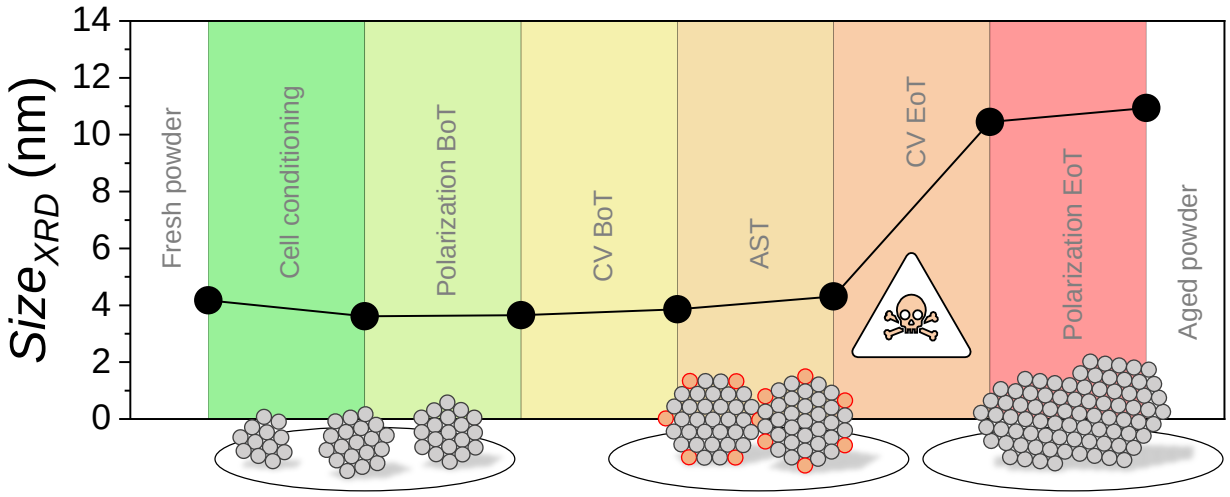

For Table of Contents Only